IL NUOVO CIMENTO **47 C** (2024) 6
DOI 10.1393/ncc/i2024-24006-3

COLLOQUIA: La Thuile 2023

W, Z, and QCD

P. CALFAYAN on behalf of the ATLAS and CMS COLLABORATIONS
Indiana University - Bloomington, IN, USA

received 10 October 2023

Summary. — The analyses of W and Z vector bosons, photon, and jets production have been carried out by the ATLAS and CMS collaborations using datasets collected during LHC Run 2, comprising from $36.3\,\text{fb}^{-1}$ to $140\,\text{fb}^{-1}$. Unfolded differential production cross sections as well as event shape observables have been measured, allowing to achieve tests of perturbative quantum chromodynamics, extractions of fundamental parameters of the Standard Model, and constraints on parton density functions.

1. – Introduction

The study of W and Z vector boson, photon, and jet production is central in the LHC physics program. The measurements of the inclusive photon (γ) and multijet (MJ) production, dominated by Quantum ChromoDynamics (QCD) processes, are indeed sensitive to the strong coupling constant (α_s) and the gluon (g) parton density function (PDF). Furthermore, the determination of the polarisation of τ leptons in $\text{Z} \to \tau\tau$ decays allows to infer the weak mixing angle ($\sin^2\theta_W^{eff}$), and rarer processes, such as the production of a W boson in association with a c-quark, enable to constrain the s-quark PDF. The accurate understanding of the processes above is also crucial in that they constitute important backgrounds to searches beyond the SM and to Higgs boson measurements, and provide substantial input to simulations. Recent results from both the ATLAS [1] and CMS [2] experiments are presented in this document.

2. – Tests of perturbative quantum chromodynamics

2˙1. *Inclusive photon production.* – The measurement of the cross section of the inclusive photon production has been performed by ATLAS using $139\,\text{fb}^{-1}$ of data at 13 TeV [3]. Photons can be produced via direct and fragmentation processes, primarily via $qg \to q\gamma$, which provides a cleaner environment than MJ events, with less hadronisation effects. This makes it a good channel to probe perturbative QCD, and to constrain the g PDF.

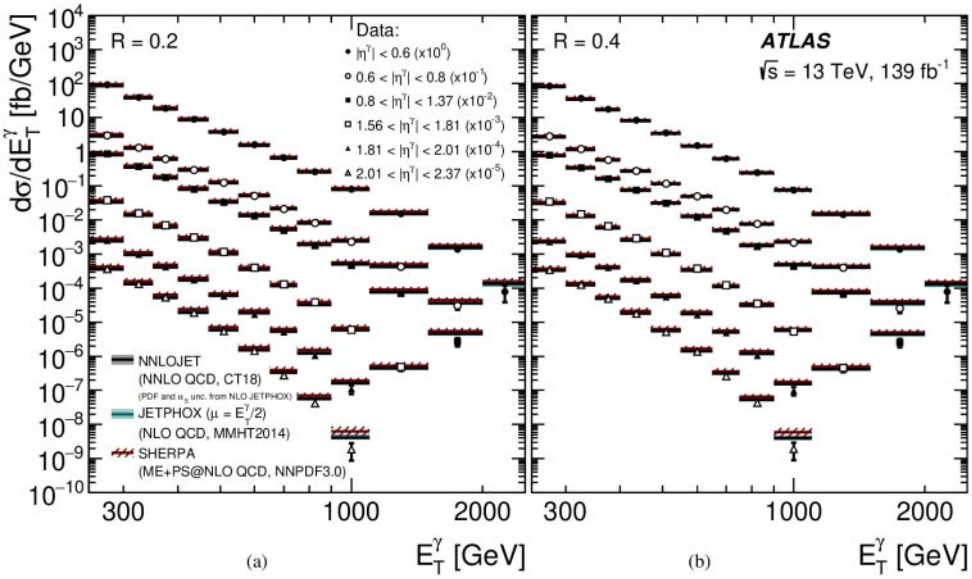

Fig. 1. – (ATLAS inclusive photon analysis [3].) Measured differential cross section of the inclusive photon production as function of the energy and pseudorapidity of the photon. Two isolation cone radii are considered. Results are compared to simulations with different accuracies in QCD.

Photon isolation is necessary to separate the final state from neutral hadron decays, so that the energy around the photon in a fixed cone with a radius $R = 0.4$ or $R = 0.2$ is considered. The main background originates from MJ events with a mis-identified photon, which is estimated using regions of data enriched in such events.

The cross section is measured as function of the energy of the photon and its pseudorapidity, and is further unfolded to particle level. Comparisons to predictions from SHERPA2.2.2 [4], as well as JETPHOX [5, 6] and NNLOJET [7] with corrected parton level, all show good modelling overall, as can be seen in fig. 1, in the case of two isolation cone radii (R). The ratio of the cross sections assuming $R = 0.2$ and $R = 0.4$ is also measured, and is well described by the NNLO prediction from NNLOJET.

2˙2. *Event shape observables in multijet events.* – Event shape observables are defined from the final state particles to characterise the hadronic energy flow. ATLAS measured the Transverse Energy-Energy Correlations (TEEC) and their azimuthal (ϕ) asymmetries (ATEEC) [8], as well as event isotropy variables [9], using MJ events in 139 fb^{-1} of data at 13 TeV. These variables have been analysed as function of H_{T2}, the scalar sum of the transverse momentum (p_T) of the two leading jets.

The TEEC quantifies the sum of the azimuthal differences between jet pairs, weighted by their transverse energy. It is infrared-safe and sensitive to g radiation. The ATEEC is the difference between the forward and backward components of TEEC, such that it cancels uncertainties symmetric in $\cos\phi$. These observables were unfolded and compared to NNLO simulations (corrected parton level) using OpenLoops2 [10], FivePointAmplitudes [11], and PentagonFunctions++ [12] for the first time, exhibiting a very good overall agreement, as depicted in fig. 2.

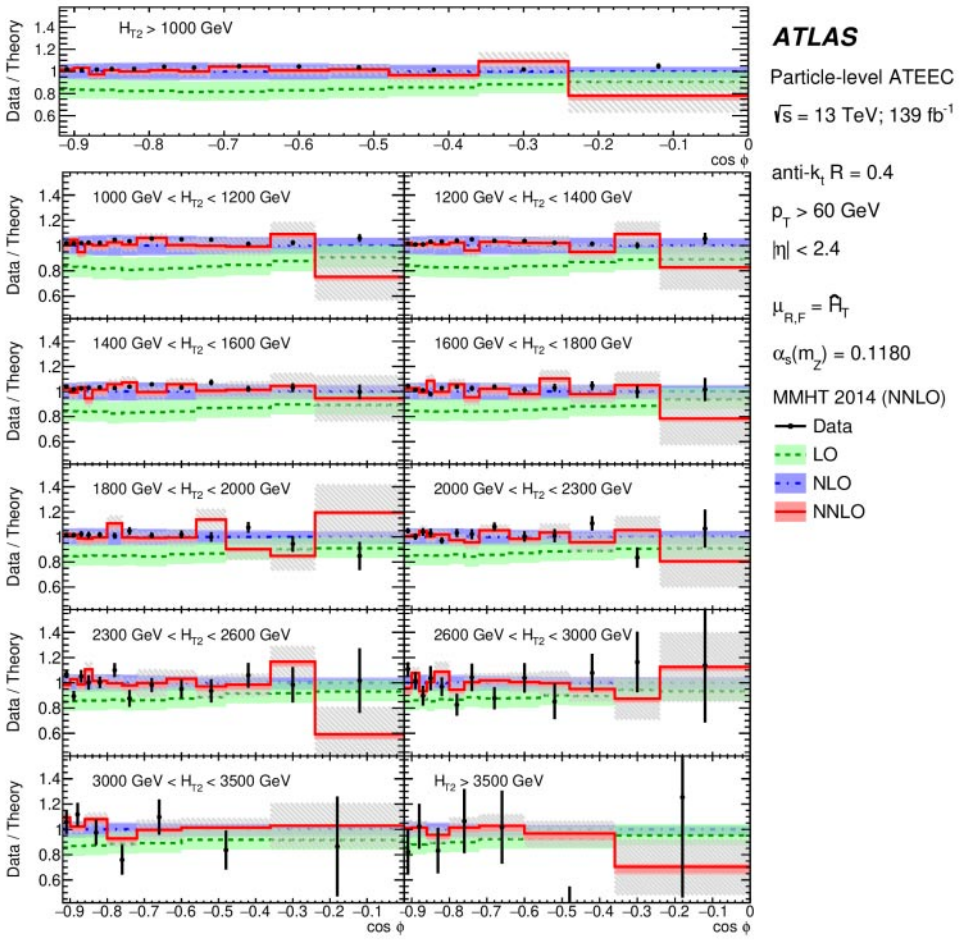

Fig. 2. – (ATLAS TEEC analysis [8].) Ratio of the ATEEC measured in data to the NLO prediction, together with the ratios of the LO and NNLO calculations to the NLO one. ATEEC is provided as function of $\cos\phi$ and H_{T2}, with ϕ the angle in the transverse plane between a pair of jets, and H_{T2} the scalar sum of the p_T of the two leading jets.

Event isotropy variables measure the distance between collider events and an isotropic reference radiation pattern in terms of Energy-Mover's distance [13]. They are infrared and colinear-safe, sensitive to isotropic events, and allow to probe phase spaces with specific QCD topologies. ATLAS determined unfolded MJ production cross sections as function of three event isotropy variables with either ring or cylindric patterns, namely I^2_{ring}, $1 - I^{128}_{ring}$, and $1 - I^{16}_{cyl}$, with 2, 128, and 16 reference points, respectively. I^2_{ring}, shown in fig. 3, compares events to a dijet topology (at low values), and is well modelled for any H_{T2} value. $1 - I^{128}_{ring}$ compares events to an isotropic MJ topology (at high values), with a prediction that degrades with increasing jet multiplicity, as can been seen by comparing fig. 5 and 6. Finally, $1 - I^{16}_{cyl}$, which compares events to a forward dijet topology and to events evenly populated in the η-ϕ plane (at high values), is not well modelled, as illustrated in fig. 4. In general, the simulations achieve a good description in the least isotropic regions, such as balanced, dijet-like arrangements.

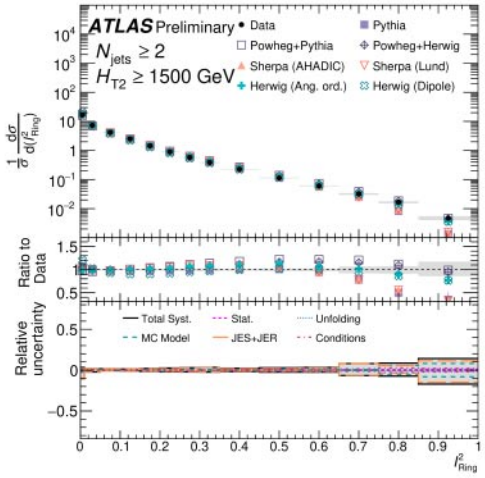

Fig. 3. – (ATLAS event isotropies analysis [9].) Differential unfolded cross section of multijet production as function of I^2_{ring}, at high H_{T2}.

2˙3. *Multidimensional cross section of dijet production.* – The production cross section of dijet events has been measured and unfolded to particle-level by CMS, based on $36.3\,\text{fb}^{-1}$ of data at 13 TeV [14]. The results are provided as function of two or three dijet system kinematic variables among its mass, its average p_T, its total boost, the rapidity of the outermost jet, and the rapidity separation of the jet pair.

The cross sections are compared to a corrected parton-level NNLO prediction using NNLOJET [15] interfaced to FASTNLO [16, 17] via APPLFAST [18, 19], with lead-color and flavour-number approximation, and electroweak corrections up to 20% at high dijet mass. Simulations show a good modelling overall, except in the ends of the energy spectra and

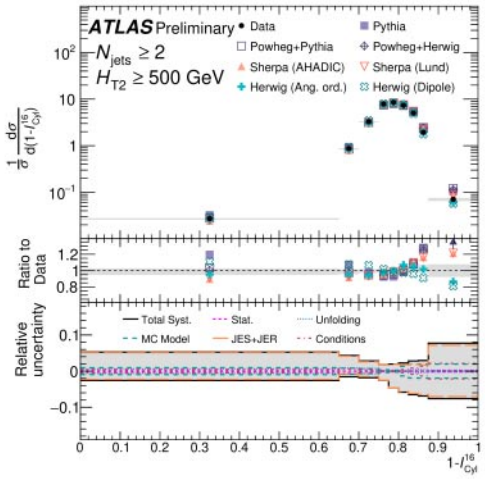

Fig. 4. – (ATLAS event isotropies analysis [9].) Differential unfolded cross section of multijet production as function of $1 - I^{16}_{cyl}$.

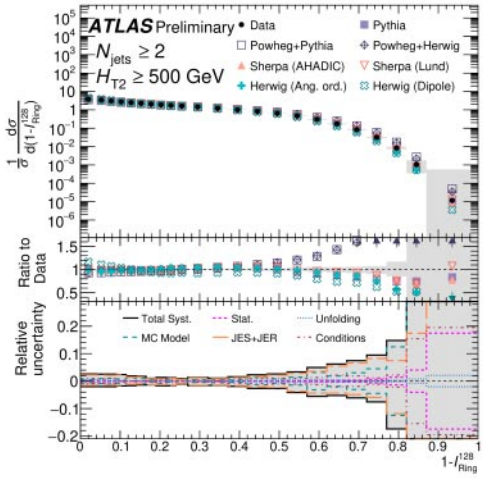

Fig. 5. – (ATLAS event isotropies analysis [9].) Differential unfolded cross section of multijet production as function of $1 - I^{128}_{ring}$, at low jets multiplicity.

in outer rapidity regions. Cross sections determined using jets with a distance parameter of $R = 0.8$ are better described than in the case $R = 0.4$, as highlighted in fig. 7 and 8, respectively.

3. – Measurements of parameters of the Standard Model

3˙1. *Strong coupling constant in multijet events.* – The ATLAS TEEC analysis [8] of MJ events and the CMS measurement of the dijet production cross section [14] both performed an extraction of the strong coupling constant α_s.

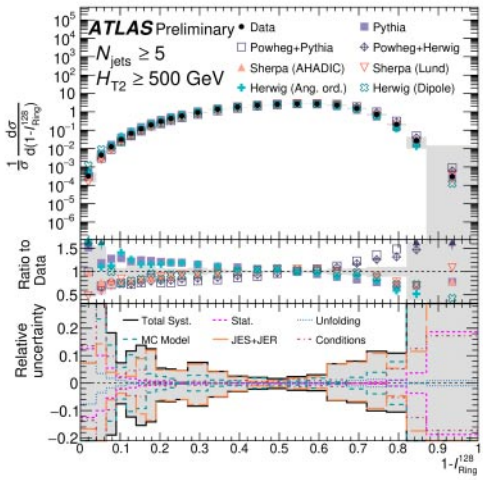

Fig. 6. – (ATLAS event isotropies analysis [9].) Differential unfolded cross section of multijet production as function of $1 - I^{128}_{ring}$, at high jets multiplicity.

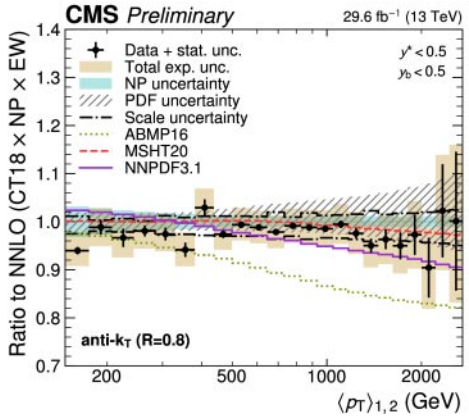

Fig. 7. – (CMS dijet analysis [14].) Measured unfolded cross section of dijet event production as function of the average p_T of the dijet system, at low dijet boost and rapidity separation. Jets are reconstructed with a distance parameter $R = 0.8$. Results are compared to a NNLO prediction.

The CMS result is determined at the Z pole mass, using a simultaneous fit together with a PDF parametrisation to account for the correlation with the g PDF. Assuming the PDF set MMHT2004, α_s is found to be 0.1201 ± 0.0020, based on three-dimensional cross section measurements.

The ATLAS result is derived in each H_{T2} interval, with different PDF sets. Assuming MMHT2004, the most accurate measurement is obtained by considering the ATEEC observable, and amounts to $0.1185^{+0.0027}_{-0.0015}$, with the theoretical uncertainty dominating. Figures 9 and 10 show α_s as function of H_{T2} using different PDF sets and from several experiments, respectively.

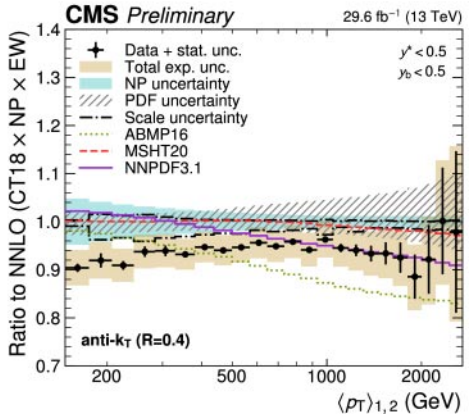

Fig. 8. – (CMS dijet analysis [14].) Measured unfolded cross section of dijet event production as function of the average p_T of the dijet system, at low dijet boost and rapidity separation. Jets are reconstructed with a distance parameter $R = 0.4$. Results are compared to a NNLO prediction.

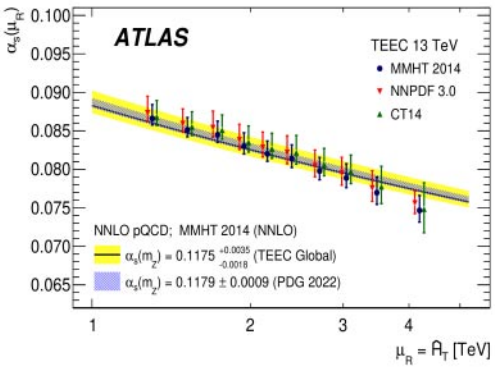

Fig. 9. – (ATLAS TEEC analysis [8].) Strong coupling constant α_s measured in each bin of H_{T2}, using different PDF sets.

3˙2. *τ lepton polarisation.* – The polarisation of the τ lepton has been measured by CMS using $36.3\,\text{fb}^{-1}$ of data at 13 TeV [20]. The analysis is considering events where the Z boson decays to τ pairs. Both leptonic and hadronic τ decays are utilised, leading to 11 channels, each being associated to an optimised observable sensitive to the τ helicity.

The main background from the SM is due to the mis-identification of hadronic τ (τ_h) in MJ and W+jets events. It is estimated from regions of data enriched in mis-identified τ_h.

The average τ polarisation $\langle P_\tau \rangle$ for a τ pair mass within 75 and 120 GeV is extracted from a global fit to data of signal and background templates for the 11 observables, distinguishing between the signal helicity states $\text{Z} \to \tau_L^- \tau_R^+$ and $\text{Z} \to \tau_R^- \tau_L^+$. The measurements of $\langle P_\tau \rangle$ from the different categories and their combination is summarised in fig. 11. The estimate of $\langle P_\tau \rangle$ corrected to its value at the Z pole amounts to -0.144 ± 0.015, which is the negative of the asymmetry parameter A_τ. The latter is compared to results from other experiments in fig. 12. In the limit where vector couplings are negligible with respect to axial-vector couplings for the initial-state fermions, the weak mixing angle can be expressed as function of $\langle P_\tau \rangle$, which allows to derive $\sin^2 \theta_W^{eff} = 0.2319 \pm 0.008\,(\text{stat}) \pm 0.018\,(\text{syst})$.

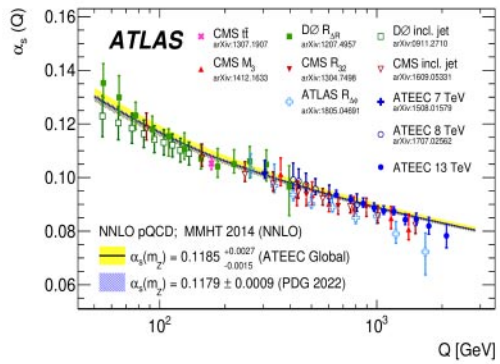

Fig. 10. – (CMS dijet analysis [14].) Strong coupling constant α_s measured in each bin of H_{T2}, compared to results from other experiments and ATLAS analyses.

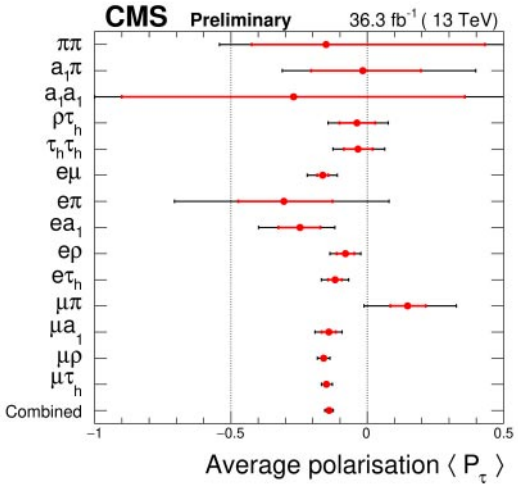

Fig. 11. – (CMS τ polarisation analysis [20].) Measurement of the average τ polarisation $\langle P_\tau \rangle$ for a τ pair mass within 75 and 120 GeV. Results from all the decay channels and their combination are included.

4. – Constraints on parton density functions

4˙1. *Measurement of W + c-jet.* – The measurement of the W boson production in association with a jet originating from a c-quark has been carried out by CMS based on 138 fb^{-1} of data at 13 TeV [21]. This analysis relies on the identification of the c-quark via the reconstruction of a c-jet and exploits 4 independent channels including the electron and muon decays of the W, as well as two orthogonal c-jet selections. The c-jet is either tagged by a muon inside a jet from a semileptonic c decay, or by the reconstruction of a secondary vertex inside a jet.

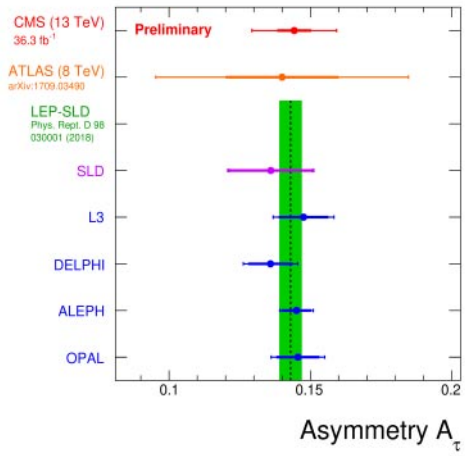

Fig. 12. – (CMS τ polarisation analysis [20].) Measurement of the asymmetry parameter A_τ compared to results from other experiments.

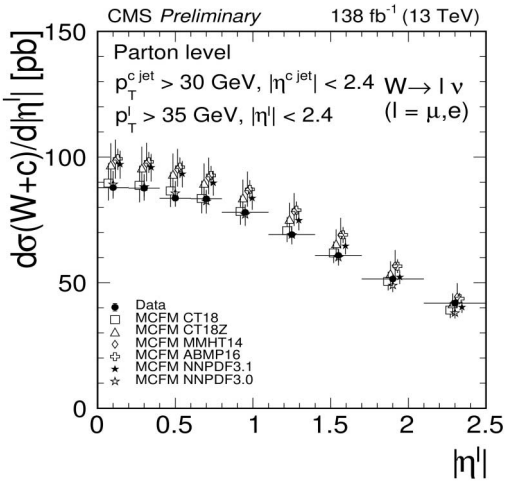

Fig. 13. – (CMS W+c analysis [21].) Unfolded cross section of the W+c production as function of the pseudorapidity of the selected lepton. Results are compared to NLO prediction.

The dominant background from the SM is due to the $\mathrm{W} + c\bar{c}$ and $t\bar{t}$ productions, which are suppressed by subtracting events where the tagged c-jet and the selected lepton have the same electric charge. The surviving contribution from the $t\bar{t}$ process is constrained from data. The selection of events with an identified semi-leptonic c-decay is affected by the remaining Z boson production in association with jets, which is also constrained from data.

The $\mathrm{W} + c$ production cross section unfolded to parton-level is shown in fig. 13 as function of the pseudorapidity of the selected lepton, and is in good agreement with the prediction from MCFM [22] at NLO in QCD. As highlighted in fig. 14, the ratio of the $\mathrm{W}^+ + c$ and $\mathrm{W}^- + c$ cross sections was determined, and amounts to $0.950 \pm 0.005\,(\mathrm{stat}) \pm$

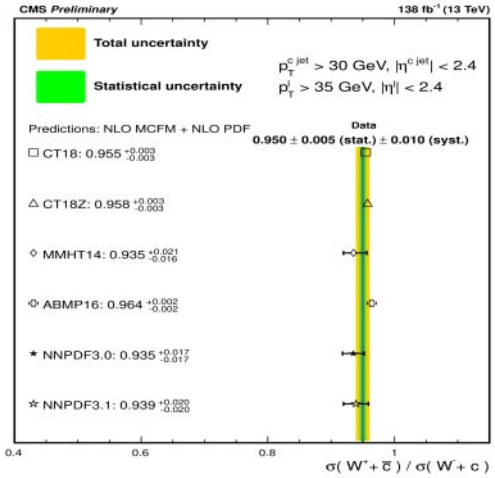

Fig. 14. – (CMS W+c analysis [21].) Measured ratio of the $\mathrm{W}^+ + c$ and $\mathrm{W}^- + c$ cross sections. Results are compared to NLO prediction, assuming different PDF sets.

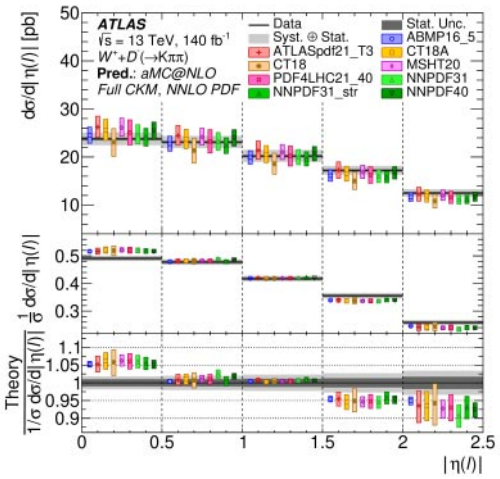

Fig. 15. – (ATLAS W + charmed hadron analysis [23].) Unfolded cross section of the $W^+ + D^-(\to K\pi\pi)$ production as function of the pseudorapidity of the lepton from the W decay. Results are compared to NLO prediction.

0.010 (syst). Simulations with various PDF assumptions model well the measurement from data, however, the PDF sets CT18 and ABMP16, which assume $s = \bar{s}$, lead to smaller uncertainties.

4·2. *Measurement of W + charmed hadron.* – The production cross section of the W boson in association with a c-quark was also measured by ATLAS, relying on 140 fb^{-1} of data at 13 TeV [23], yet with another strategy. The c-quark is indeed identified via the reconstruction of a charmed hadron $D^{(*)}$ using the mass of the secondary vertex. The meson decays $D^{\pm} \to K^{\mp}\pi^{\pm}\pi^{\pm}$ and $D^{*\pm} \to D^0\pi^{\pm} \to (K^{\mp}\pi^{\pm})\pi^{\pm}$, as well as both the electron and muon decays of the W, are considered.

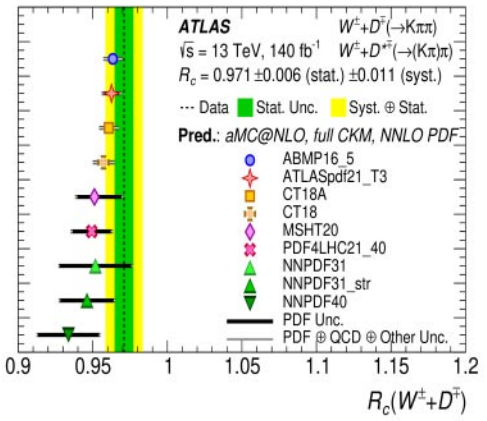

Fig. 16. – (ATLAS W + charmed hadron analysis [23].) Measured ratio R_c of the $W^+ + D^{(*)-}$ and $W^- + D^{(*)+}$ cross sections. Results are compared to NLO prediction, assuming different PDF sets.

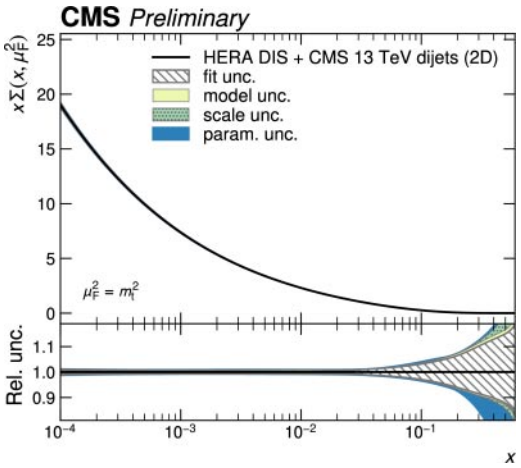

Fig. 17. – (CMS dijet analysis [14].) Measured PDF of the total sea quarks as function of the parton momentum fractions x. The impact of different sources of uncertainties is provided. Results from CMS and HERA experiments [25] are combined.

By contrast to the backgrounds from the SM, the selected lepton and meson have opposite electric charges in signal events, which is exploited to enhance the latter. The main background is due to tracks in the reconstructed secondary vertex that are partly or completely not corresponding to the $\mathrm{W} + D^{(*)}$ candidate. Contributions from top quark and MJ events are constrained from data.

The unfolded measurement of the $\mathrm{W}^+ + D^-$ production cross section as function of the pseudorapidity of the selected lepton is shown in fig. 15, while the ratio R_c of the $\mathrm{W}^+ + D^{(*)-}$ and $\mathrm{W}^- + D^{(*)+}$ cross sections is depicted in fig. 16. Both agree with the NLO prediction from aMC@NLO [24] for various PDF assumptions. R_c is however determined with a higher accuracy when using the PDF set CT18, AMBP16, or ATLASpdf21, which all assume $s = \bar{s}$. This suggests that the s-$\bar{s}$ asymmetry is small.

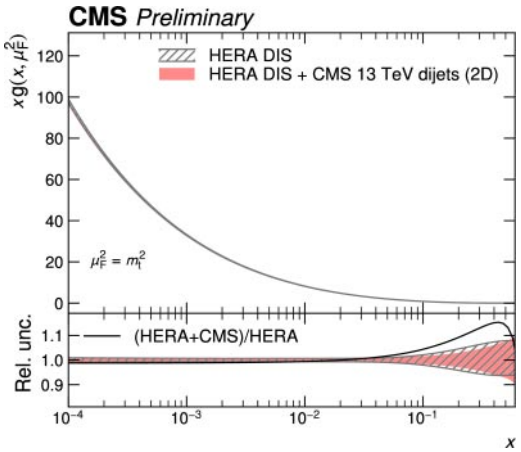

Fig. 18. – (CMS dijet analysis [14].) Measured PDF of the g as function of the parton momentum fractions x. Results from HERA experiments [25] are compared to the combination with those from CMS.

4˙3. *PDF constraints in dijets events.* – The analysis from CMS performing the measurement of the dijet production cross section [14] also achieved a PDF fit including results from deep inelastic scattering (DIS) in $e^{\pm}p$ collisions at the HERA collider [25].

The two-dimensional cross section measurements involving a jet distance parameter $R = 0.8$ provided the best precision to constrain the PDF of the g, as well as of the u- and d-quarks. The uncertainties originating from the fit, the non-PDF parameters, the alternative parametrisation, and the scale variation were accounted for, as can be seen in fig. 17 for the PDF of the total sea quarks. An overall improvement of the PDF precision is achieved, especially for the g PDF when the parton momentum fraction x exceeds 0.1, as shown in fig. 18.

5. – Conclusion

Unfolded differential production cross sections as well as event shape variables have been determined considering various processes of the SM, allowing to probe perturbative QCD effects, to measure fundamental SM parameters (α_s, $\sin^2\theta_W^{eff}$), and to constrain PDF. Accurate measurements were carried out based on data with integrated luminosities up to the complete statistics of LHC Run 2. Specific final states were analysed, involving data-driven techniques to constrain background processes when simulation was not sufficient.

* * *

This material is based upon work supported by the U.S. Department of Energy, Office of Science, Office of High Energy Physics, under Award Number DE-SC0010120.

REFERENCES

[1] ATLAS Collaboration, *J. Instrum.*, **3** (2008) S08003.
[2] CMS Collaboration, *J. Instrum.*, **3** (2008) S08004.
[3] ATLAS Collaboration, CERN-EP-2022-247, arXiv:hep-ex/2302.00510.
[4] Bothmann E. *et al.*, *SciPost Phys.*, **7** (2019) 034.
[5] Catani S. *et al.*, *J. High Energy Phys.*, **05** (2002) 028.
[6] Aurenche P. *et al.*, *Phys. Rev. D*, **73** (2006) 094007.
[7] Chen X. *et al.*, *J. High Energy Phys.*, **08** (2022) 094.
[8] ATLAS Collaboration, CERN-EP-2022-282, arXiv:hep-ex/2301.09351.
[9] ATLAS Collaboration, ATLAS-CONF-2022-056.
[10] Buccioni F. *et al.*, *Eur. Phys. J. C*, **79** (2019) 866.
[11] Abreu S. *et al.*, *J. High Energy Phys.*, **07** (2021) 95.
[12] Chicherin D. and Sotnikov V., *J. High Energy Phys.*, **12** (2020) 167.
[13] Komiske T., Metodiev E. M. and Thaler J., *Phys. Rev. Lett.*, **123** (2019) 041801.
[14] CMS Collaboration, CMS-PAS-SMP-21-008.
[15] Gehrmann T. *et al.*, *PoS*, **RADCOR2017** (2018) 074, arXiv:hep-ph/1801.06415.
[16] Kluge T. *et al.*, in *Proceedings, DIS 2006* (World Scientific) 2007, arXiv:hep-ph/0609285.
[17] Britzger D. *et al.*, in *Proceedings, DIS 2012* (DESY) 2012, arXiv:hep-ph/1208.3641.
[18] Britzger D. *et al.*, *Eur. Phys. J. C*, **79** (2019) 845.
[19] Britzger D. *et al.*, *Eur. Phys. J. C*, **82** (2022) 930.
[20] CMS Collaboration, CMS-PAS-SMP-18-010.
[21] CMS Collaboration, CMS-PAS-SMP-21-005.
[22] Campbell J. and Neumann T., *J. High Energy Phys.*, **12** (2019) 034.
[23] ATLAS Collaboration, CERN-EP-2022-291, arXiv:hep-ex/2302.00336.
[24] Alwall J. *et al.*, *J. High Energy Phys.*, **07** (2014) 079.
[25] H1 and ZEUS Collaborations, *Eur. Phys. J. C*, **75** (2015) 580.